Analytical Evaluation of the Asymptotic Impedance Matrix of Asymmetric Gap Discontinuities

Seong-Ook Park, *Member, IEEE,* and Constantine A. Balanis, *Fellow, IEEE*

***Abstract*— New analytical formulas have been developed for evaluating the asymptotic impedance matrix of an asymmetric gap by using the integral transform method. Application of the newly derived formulas shows a dramatic improvement of the computation time for evaluating the overall impedance-matrix elements for the symmetric and asymmetric gaps while retaining the accuracy.**

***Index Terms*— Discontinuities, integral equation, spectral-domain method.**

I. Introduction

ASYMMETRIC gap discontinuities on a grounded dielectric slab have numerous applications in monolithic microwave integrated circuits (MMIC's), such as in filters and impedance transformers, and interface well with active devices. Accurate analysis of asymmetric gap discontinuities is a more computationally time-intensive problem than that of symmetric gaps because if the width of the two electrical narrow strip lines is mismatched, the integrand of each interaction matrix of an asymmetric gap is more highly oscillatory compared to those of a symmetric gap.

In order to speed up the execution time, this paper presents an analytical technique for solving the asymptotic part of the impedance matrix of general asymmetric gap problems. If two strips have an equal width, a symmetric gap is a special case of an asymmetric one. To verify the efficiency and accuracy of the proposed method, the newly derived formulas were applied to two cases: a symmetric and an asymmetric gap.

II. Theory

The asymmetric gap in open microstrip structures is subject to radiation at discontinuities in the form of either space or surface waves. A full-wave solution is needed to take into account such phenomena. An asymmetric gap discontinuity on a grounded dielectric substrate is depicted in Fig. 1. Full-wave analysis of gap discontinuities, by considering both the transverse and longitudinal current components, was reported by Jackson [1] and Alexópoulos [2]. However, for electrically narrow strips, the transverse current component can be neglected to simplify the solution of the full-wave equation; thus, only a longitudinal current component is considered for the analysis of an asymmetric gap. The electric field due to the current densities on the left and right strips can be expressed as [3]

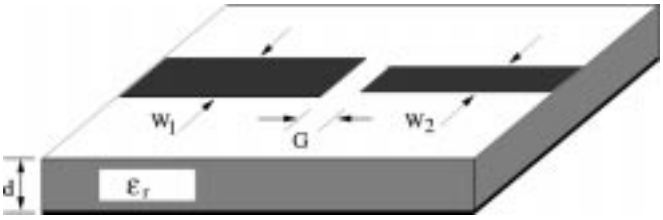

Fig. 1. Geometry of asymmetric gap discontinuities.

$$E_x(x,y) = \frac{1}{4\pi^2}\int_{-\infty}^{\infty}\int_{-\infty}^{\infty}\tilde{G}_{xx}(k_x,k_y) \cdot[\tilde{J}_x^{\text{Left}}(k_x,k_y) + \tilde{J}_x^{\text{Right}}(k_x,k_y)]\cdot e^{-j(k_x x + k_y y)}\,dk_x\,dk_y \tag{1}$$

where $\tilde{G}_{xx}$ is the $\hat{x}$ component of the dyadic Green's function due to an $\hat{x}$-directed infinitesimal dipole, and $\tilde{J}_x^{\text{Left}}$ and $\tilde{J}_x^{\text{Right}}$ represent the spectral-domain current densities on the left and right strips, respectively.

The current density on the left line is modeled as a standing wave (sum of incident and reflection wave) with expansion functions of the form

$$J_x^{\text{Left}}(x,y) = J_x^{\text{inc}}(x,y) + J_x^{\text{ref}}(x,y) + \sum_{m=1}^{M} I_m J_{xm}(x,y) \tag{2}$$

$$J_x^{\text{inc}}(x,y) = \frac{e^{-jk_{e_1}x}}{\sqrt{1-(2y/W_1)^2}} \tag{3}$$

$$J_x^{\text{ref}}(x,y) = -R\frac{e^{jk_{e_1}x}}{\sqrt{1-(2y/W_1)^2}}, \qquad x \le 0, |y| \le \frac{W_1}{2} \tag{4}$$

where k_{e_1} is the effective propagation constant of an infinite strip line with width W_1, and R is the reflection coefficient to be determined.

Manuscript received May 15, 1997; revised January 19, 1998. This work was supported by the U.S. Army Research Office under Contract DAAL 03-92-G-0262.

S.-O. Park was with the Department of Electrical Engineering, Telecommunications Research Center, Arizona State University, Tempe, AZ 85287-7206 USA. He is now with the Information and Communications University, Taejon 305-350, Korea.

C. A. Balanis is with the Department of Electrical Engineering, Telecommunications Research Center, Arizona State University, Tempe, AZ 85287-7206 USA.

Publisher Item Identifier S 0018-9480(98)05506-9.

0018–9480/98$10.00 © 1998 IEEE

On the right strip line, the current density is represented as a traveling wave with expansion functions of the form

$$J_x^{\text{Right}}(x,y) = J_x^{\text{tran}}(x,y) + \sum_{p=1}^{P} I_p J_{xp}(x,y) \tag{5}$$

$$J_x^{\text{tran}}(x,y) = T\frac{e^{-jk_{e_2}(x-G)}}{\sqrt{1-(2y/W_2)^2}}, \qquad x \geq G, |y| \leq \frac{W_2}{2} \tag{6}$$

where k_{e_2} is the effective propagation constant of an infinite strip line with width W_2, and T is the transmission coefficient to be determined.

Each current density of the standing- and traveling-wave modes can be decomposed into semi-infinite sine and cosine wave terms. The semi-infinite cosine expansion mode starts at a quarter-wavelength away from the gap discontinuity to satisfy the boundary condition at the end of the line. Doing this, the current densities on each strip line can be expressed as

$$J_x^{\text{inc}} + J_x^{\text{ref}} = \left[(1-R)\cdot f_{s_1}\left(k_{e_1}x + \frac{\pi}{2}\right) - j(1+R) \cdot f_{s_1}(k_{e_1}x)\right] \Big/ \sqrt{1-(2y/W_1)^2} \tag{7}$$

$$J_x^{\text{tran}} = \left[-T\cdot f_{s_2}\left(k_{e_2}[x-G] + \frac{\pi}{2}\right) - jT \cdot f_{s_2}(k_{e_2}[x-G])\right] \Big/ \sqrt{1-(2y/W_2)^2} \tag{8}$$

where

$$f_{s_1}(u) = \begin{cases} \sin(u), & \text{if } -M\pi < u < 0 \\ 0, & \text{if otherwise} \end{cases} \tag{9}$$

$$f_{s_2}(u) = \begin{cases} \sin(u), & \text{if } M\pi > u > 0 \\ 0, & \text{if otherwise.} \end{cases} \tag{10}$$

The current density components of the standing and traveling waves have ideally semi-infinite ranges. However, for convenience of numerical evaluations, these sinusoidal-type currents are truncated after several integer numbers of half-wavelength. Typically, the convergence of the solution is achieved if M in (9) and (10) is greater than six [3], [4]. In this paper, we use $M = 8$.

Expansion functions J_{xm} and J_{xp} in (2) and (5) use the following triangular form:

$$\Lambda\left(\frac{x-x_u}{L_i}\right) = \begin{cases} 1 - \dfrac{|x-x_u|}{L_i}, & |x-x_u| < L_i \\ 0, & \text{otherwise} \end{cases} \tag{11}$$

where u and i have m and one for the left signal line, and p and two for the right signal line.

The current expansions for an asymmetric gap are shown in Fig. 2. Electric-field boundary condition (i.e., the total $\hat{x}$-directed electric field due to the entire current on the conductor strip is equal to zero) is employed on the conductor strip. The electric-field integral equation can be converted into a matrix system by multiplying by a testing function and integrating the inner product over the support of this function. Since there are $(M+P+2)$ unknown coefficients, one additional weighting function on each side of the signal line is needed. Therefore, starting from the gap discontinuity, we have $(M+1)$ triangular

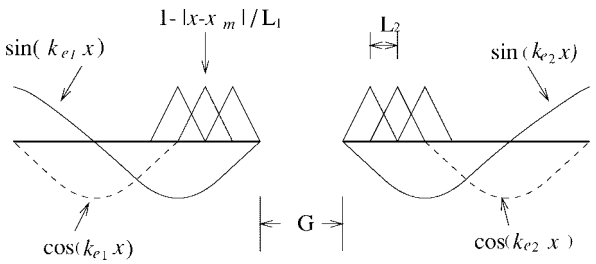

Fig. 2. Current expansions on the asymmetric gap.

weighting functions on the left signal line and $(P+1)$ triangular weighting functions on the right signal line [3]. This procedure leads to the following matrix system with $M+P+2$ unknowns:

$$\begin{bmatrix} [Z_{mn}] & [Z_{mc}+jZ_{ms}] & [Z_{mq}] & [Z_{\text{mtc}}+jZ_{\text{mts}}] \\ [Z_{pn}] & [Z_{pc}+jZ_{ps}] & [Z_{pq}] & [Z_{\text{ptc}}+jZ_{\text{pts}}] \end{bmatrix} \begin{bmatrix} [I_n] \\ -R \\ [I_q] \\ T \end{bmatrix} = \begin{bmatrix} [-Z_{mc}+jZ_{ms}] \\ [-Z_{pc}+jZ_{ps}] \end{bmatrix}. \tag{12}$$

Each submatrix in (12) represents a set of mutual interactions between the test and basis functions. Their respective mathematical representations and asymptotic forms of each submatrix are presented in [5, Appendix B]. Since the integrand of the double infinite integration in each submatrix element converges slowly with a highly oscillatory behavior, numerical integration is extremely laborious. Thus, the analytical procedures of the asymptotic part of impedance matrix, if applicable, can considerably reduce the computational effort involving Sommerfeld-type integrals.

III. Analytical Methods of the Asymptotic Impedance Matrix

The asymptotic part of submatrices Z_{mn} and Z_{pq} can be transformed into a finite one-dimensional integral by using the same procedures described in [6]. Their results also have similar formulas as in [6, eqs. (18) and (19)]. The asymptotic part of submatrices Z_{mq} and Z_{pn} have the following two general forms represented by

$$I_{mq}^a = \int_0^\infty \int_0^\infty \frac{\cos(d_s k_x)}{\sqrt{k_x^2+k_y^2}} \frac{\sin^2(k_x L_1/2)}{k_x^2} \cdot \frac{\sin^2(k_x L_2/2)}{k_x^2} J_0\left(k_y\frac{W_1}{2}\right) J_0\left(k_y\frac{W_2}{2}\right) dk_x\, dk_y \tag{13}$$

$$I_{mq}^b = \int_0^\infty \int_0^\infty \frac{\cos(d_s k_x)}{\sqrt{k_x^2+k_y^2}} \sin^2(k_x L_1/2) \cdot \frac{\sin^2(k_x L_2/2)}{k_x^2} J_0\left(k_y\frac{W_1}{2}\right) J_0\left(k_y\frac{W_2}{2}\right) dk_x\, dk_y. \tag{14}$$

Other remaining submatrices, such as Z_{mc}, Z_{ms}, $Z_{pc}Z_{ps}$, Z_{mtc}, Z_{mts}, Z_{ptc}, and Z_{pts} involve the following two general

asymptotic forms represented by:

$$I^a_{\rm mcs} = \int_0^\infty \int_0^\infty \frac{\cos(d_s k_x)}{\sqrt{k_x^2+k_y^2}} \frac{\sin^2(k_x L_i/2)}{k_x^2(k_x^2-k_{e_l}^2)} \cdot J_0\left(k_y \frac{W_i}{2}\right) J_0\left(k_y \frac{W_l}{2}\right) dk_x\, dk_y \tag{15}$$

$$I^b_{\rm mcs} = \int_0^\infty \int_0^\infty \frac{\cos(d_s k_x)}{\sqrt{k_x^2+k_y^2}} \frac{\sin^2(k_x L_i/2)}{k_x^2-k_{e_l}^2} \cdot J_0\left(k_y \frac{W_i}{2}\right) J_0\left(k_y \frac{W_l}{2}\right) dk_x\, dk_y \tag{16}$$

where i and l have one for the left signal line, and two for the right signal line.

With the aid of [6, eq. (11)], the integrals of (13)–(16) can be rewritten as (17)–(20), shown at the bottom of this page. Analytical integration of (17)–(20) with respect to k_y is defined as follows:

$$B(\chi - d_s) = \int_0^\infty J_0\left(\frac{W_i}{2}k_y\right) J_0\left(\frac{W_l}{2}k_y\right) K_0(k_y|\chi - d_s|)\, dk_y \tag{21}$$

where the analytical solution of $B(\chi - d_s)$ is derived in Appendix A.

It can be easily shown that the analytical result of (21) can be reduced to [6, eq. (14)] by letting $W_i = W_l = W$. Using straightforward algebra, the second integrals in (17) and (18) with respect to k_x can be represented by

$$\mathcal{A}(\chi) = \int_0^\infty \cos(k_x\chi) \frac{\sin^2(k_x L_1/2)}{k_x^2} \frac{\sin^2(k_x L_2/2)}{k_x^2}\, dk_x = \pi \frac{L_1 L_2}{16} \int_{-\infty}^\infty \Lambda\left(\frac{x-\chi}{L_1}\right) \Lambda\left(\frac{x}{L_2}\right) dx \tag{22}$$

$$\mathcal{B}(\chi) = \int_0^\infty \cos(k_x\chi) \sin^2(k_x L_1/2) \frac{\sin^2(k_x L_2/2)}{k_x^2}\, dk_x = \pi \frac{L_1}{8}\left[\Lambda\left(\frac{x}{L_1}\right) - \frac{1}{2}\Lambda\left(\frac{x-L_2}{L_1}\right) - \frac{1}{2}\Lambda\left(\frac{x+L_2}{L_1}\right)\right] \tag{23}$$

where Λ is defined in (11).

From the above formulas, the values of the integrals in (22) and (23) are zero for $|\chi| \geq (L_1 + L_2)$. Therefore, by substituting (21)–(23) into (17) and (18), the infinite double integrals of (13) and (14) are transformed into finite one-dimensional integrals of

$$I^a_{mq} = \frac{1}{\pi} \int_{-L_1-L_2}^{L_1+L_2} B(\chi - d_s) \cdot \mathcal{A}(\chi)\, d\chi \tag{24}$$

$$I^b_{mq} = \frac{1}{\pi} \int_{-L_1-L_2}^{L_1+L_2} B(\chi - d_s) \cdot \mathcal{B}(\chi)\, d\chi. \tag{25}$$

The validity of the above two formulas is directly verified by letting $W_1 = W_2 = W$ and $L_1 = L_2 = L$. By doing this, (24) and (25) reduce to [6, eqs. (18) and (19)].

The second integrals in (19) and (20) with respect to k_x can also be analytically solved, as shown in (26) and (27), at the bottom of the next page, where the derivations of (26) and (27) are illustrated in Appendix B.

Substituting (21), (26), and (27) into (19) and (20), the infinite double integrals of (15) and (16) can each be transformed into an infinite one-dimensional integral of

$$I^a_{\rm mcs} = \frac{1}{\pi} \int_{-\infty}^\infty B(\chi - d_s) \cdot \mathcal{C}(\chi)\, d\chi \tag{28}$$

$$I^b_{\rm mcs} = \frac{1}{\pi} \int_{-\infty}^\infty B(\chi - d_s) \cdot \mathcal{D}(\chi)\, d\chi. \tag{29}$$

If the argument $|\chi - d_s|$ in (21) is greater than $[10 \cdot \max(W_1, W_2)]$, $B(\chi - d_s)$ in (21) rapidly approaches the asymptotic behavior represented by

$$\lim_{|\chi - d_s| \to \infty} B(\chi - d_s) \approx \frac{\pi}{2} \frac{1}{|\chi - d_s|} \tag{30}$$

where

$$\lim_{x \to 1} P_{-(1/2)}(x) = 1. \tag{31}$$

With the aid of (30), the infinite one-dimensional integrals of (28) and (29) can be further simplified to finite integrals of

$$I^a_{\rm mcs} \approx \frac{1}{\pi} \int_{A^L}^{A^U} B(\chi - d_s) \cdot \mathcal{C}(\chi)\, d\chi - \frac{\pi}{4k_{e_l}^3} \mathcal{H} \tag{32}$$

$$I^b_{\rm mcs} \approx \frac{1}{\pi} \int_{A^L}^{A^U} B(\chi - d_s) \cdot \mathcal{D}(\chi)\, d\chi - \frac{\pi}{4k_{e_l}} \mathcal{H} \tag{33}$$

where $\mathcal{H}$ is given in Appendix B, and A^U and A^L are given by $\max[L_i, |d_s| + 10 \cdot \max(W_1, W_2)]$ and $\min[-L_i, |d_s| - 10 \cdot \max(W_1, W_2)]$, respectively.

$$I^a_{mq} = \frac{1}{\pi} \int_{-\infty}^\infty \left\{ \int_0^\infty K_0(k_y|\chi - d_s|) J_0\left(k_y \frac{W_1}{2}\right) J_0\left(k_y \frac{W_2}{2}\right) dk_y \times \int_0^\infty \cos(k_x\chi) \frac{\sin^2(k_x L_1/2)}{k_x^2} \frac{\sin^2(k_x L_2/2)}{k_x^2}\, dk_x \right\} d\chi \tag{17}$$

$$I^b_{mq} = \frac{1}{\pi} \int_{-\infty}^\infty \left\{ \int_0^\infty K_0(k_y|\chi - d_s|) J_0\left(k_y \frac{W_1}{2}\right) J_0\left(k_y \frac{W_2}{2}\right) dk_y \times \int_0^\infty \cos(k_x\chi) \sin^2(k_x L_1/2) \frac{\sin^2(k_x L_2/2)}{k_x^2}\, dk_x \right\} d\chi \tag{18}$$

$$I^a_{\rm mcs} = \frac{1}{\pi} \int_{-\infty}^\infty \left\{ \int_0^\infty K_0(k_y|\chi - d_s|) J_0\left(k_y \frac{W_i}{2}\right) J_0\left(k_y \frac{W_l}{2}\right) dk_y \times \int_0^\infty \frac{\cos(k_x\chi)}{k_x^2 - k_{e_l}^2} \frac{\sin^2(k_x L_i/2)}{k_x^2}\, dk_x \right\} d\chi \tag{19}$$

$$I^b_{\rm mcs} = \frac{1}{\pi} \int_{-\infty}^\infty \left\{ \int_0^\infty K_0(k_y|\chi - d_s|) J_0\left(k_y \frac{W_i}{2}\right) J_0\left(k_y \frac{W_l}{2}\right) dk_y \times \int_0^\infty \frac{\cos(k_x\chi)}{k_x^2 - k_{e_l}^2} \sin^2(k_x L_i/2)\, dk_x \right\} d\chi \tag{20}$$

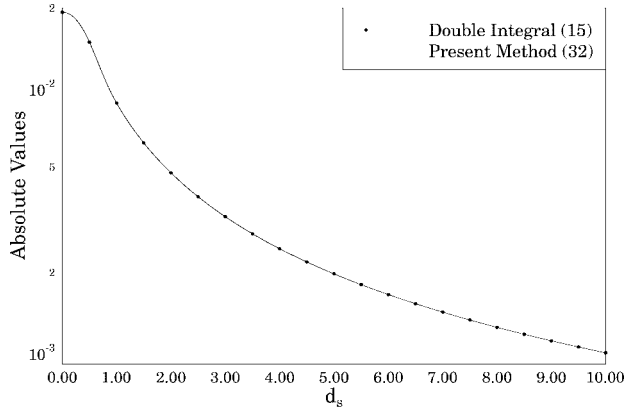

(a)

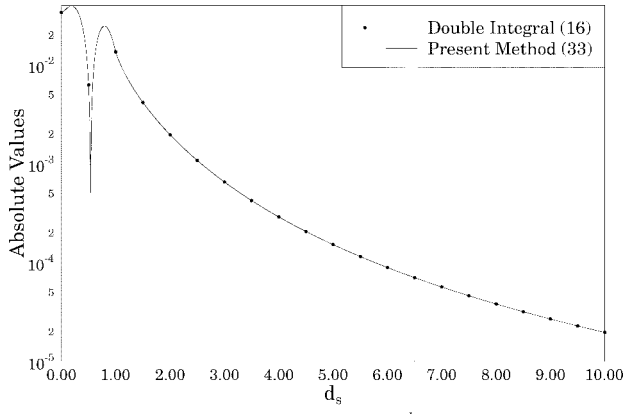

(b)

Fig. 3. The values of (a) I^a_{mcs} and (b) I^b_{mcs} for $W_1 = 1$ mm, $W_2 = 2$ mm, $L_i = 1$ mm, and $k_{e_l} = 2\pi$ rad/mm.

In order to check the validity of the two formulas in (32) and (33), the double integrals I^a_{mcs} and I^b_{mcs}, which were defined in (15) and (16), respectively, are calculated with upper limit $\beta^u = 300$ rad/mm for $W_1 = 1$ mm, $W_2 = 2$ mm, $L_i = 1$ mm, and values of d_s from $0 \leq d_s \leq 10$. The value of k_{e_l} was chosen 2π rad/mm to eliminate the singularity in (15) and (16). With these parameters, the one-dimensional integrals I^a_{mcs} and I^b_{mcs} in (32) and (33) are evaluated with an accuracy of four significant figures. These results are plotted in Fig. 3, which indicate excellent agreement. In this example, the average computation time to obtain the results of Fig. 3, using the newly derived formulas of (32) and (33), is approximately 3000 times faster than those of the two-dimensional method.

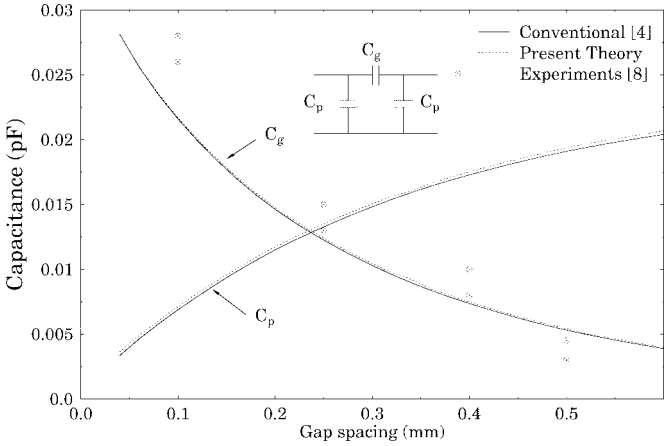

Fig. 4. Capacitance values of a symmetric gap with $\epsilon_r = 8.875$, $W_1 = W_2 = d = 0.508$ mm.

The numerical evaluations of each interaction involving the truncated sinusoidal basis function have the most time-consuming part compared to the other remaining matrix elements. Thus, the direct spectral-domain analysis (SDA) without acceleration technique has a serious limitation for this part. However, the proposed analytical technique of the tail integral considerably reduces the computation time, especially for this part.

IV. Numerical Results of Symmetric and Asymmetric Gaps

The symmetric gap discontinuity (at low frequencies) can be modeled by the equivalent circuit such as the capacitive π network. Equivalent shunt and series capacitances C_p and C_g can be extracted from the reflection coefficient Γ and the transmission coefficient T [4], [7].

The newly derived formulas are applied to the efficient evaluation of the matrix elements in (12). Fig. 4 shows the equivalent capacitance values for a symmetric gap discontinuity with $\epsilon_r = 8.875$, $W_1 = W_2 = d = 0.508$ mm, and $f = 5$ GHz as a function of gap spacing. For comparisons, the

$$\mathcal{C}(\chi) = \int_0^\infty \frac{\cos(k_x\chi)}{k_x^2 - k_{e_l}^2} \frac{\sin^2(k_x L_i/2)}{k_x^2}\, dk_x = \begin{cases} -\dfrac{\pi}{4}\dfrac{1}{k_{e_l}^3}[1 - \cos(k_{e_l}L_i)] \cdot \sin(|\chi| k_{e_l}), & \text{if } |\chi| > L_i \\ -\dfrac{\pi}{4}\dfrac{1}{k_{e_l}^3}[k_{e_l}L_i - |\chi| k_{e_l} + \sin(|\chi| k_{e_l}) - \cos(k_{e_l}|\chi|)\sin(k_{e_l}L_i)], & \text{if } |\chi| < L_i \end{cases} \tag{26}$$

$$\mathcal{D}(\chi) = \int_0^\infty \frac{\cos(k_x\chi)}{k_x^2 - k_{e_l}^2} \sin^2(k_x L_i/2)\, dk_x = \begin{cases} -\dfrac{\pi}{4k_{e_l}}[1 - \cos(k_{e_l}L_i)] \cdot \sin(k_{e_l}|\chi|), & \text{if } |\chi| > L_i \\ -\dfrac{\pi}{4k_{e_l}}[\sin(k_{e_l}|\chi|) - \sin(k_{e_l}L_i) \cdot \cos(k_{e_l}\chi)], & \text{if } |\chi| < L_i \end{cases} \tag{27}$$

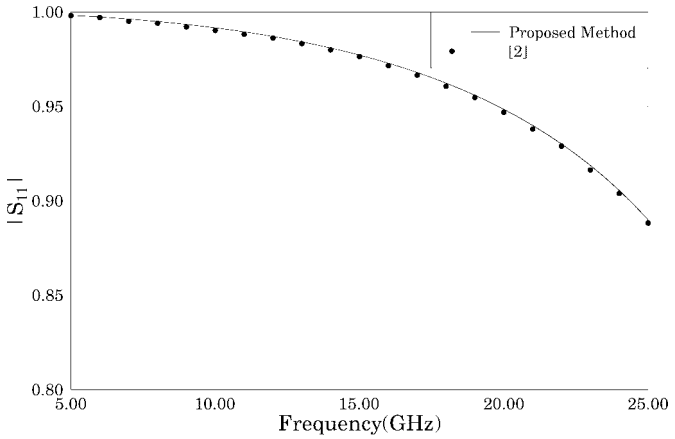

(a)

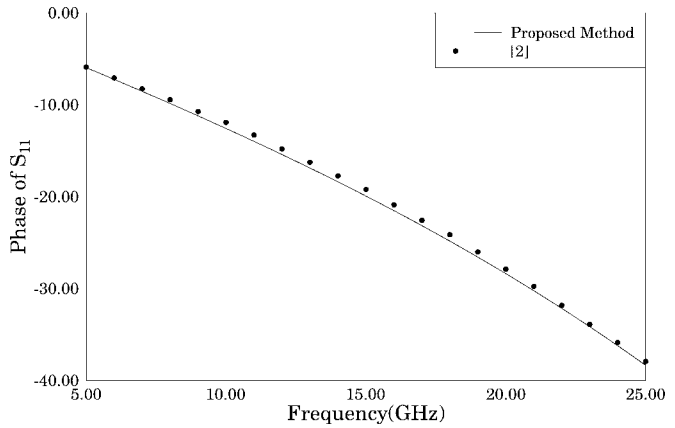

(b)

Fig. 5. Comparison of the S_{11} of a symmetric gap ($\epsilon_r = 9.9$, $d = 0.635$ mm, $W_1 = W_2 = 0.635$ mm, $G = 0.508$ mm). (a) Magnitude of S_{11}. (b) Phase of S_{11}.

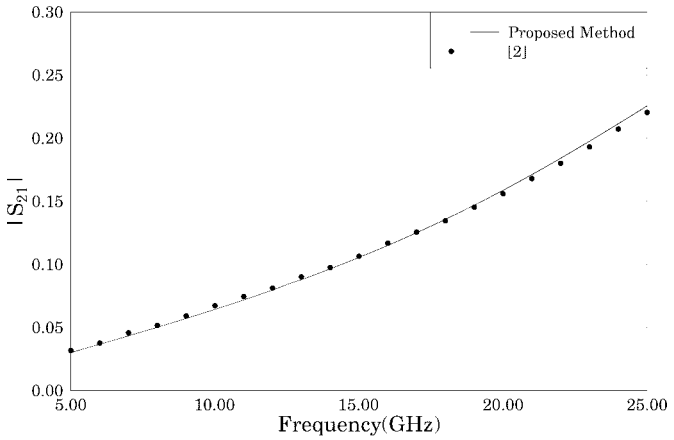

(a)

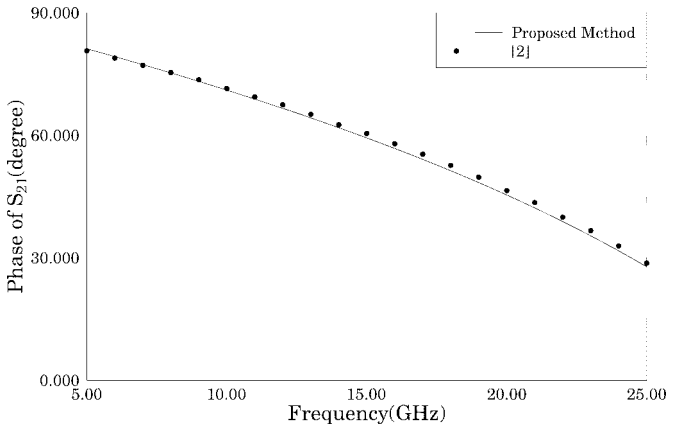

(b)

Fig. 6. Comparison of the S_{21} of a symmetric gap ($\epsilon_r = 9.9$, $d = 0.635$ mm, $W_1 = W_2 = 0.635$ mm, $G = 0.508$ mm). (a) Magnitude of S_{21}. (b) Phase of S_{21}.

results obtained by the conventional SDA using the piecewise sinusoidal basis functions [4] and those of measurements [8] are included in Fig. 4. The conventional SDA in [4] neglects the transverse current component and an upper limit $\beta^u = 400 \cdot k_0$ was used for the evaluation of the each submatrix in (12). However, the proposed method, using an upper limit of $\beta^u = 50 \cdot k_0$, is found to be sufficiently accurate. The convergence of the results is achieved by increasing the number of the basis functions to $N = P = 21$. Our results are in excellent agreement with the data obtained in [4] and seem to be in reasonably good agreement with the experimental results of [8]. The authors of [8] conducted two experiments and reported for each spacing two sets of data, which were slightly different from each other; both sets of C_g are shown in Fig. 4.

The effective propagation constant k_{e_l} corresponds to the mode that actually propagates in the transmission line with a known analytical variation of the assumed current density along the transverse direction. Usually, the value of k_{e_l} can be precisely evaluated by using the numerical methods introduced in [1] and [3]. In these results, k_{e_l} was obtained with the accuracy up to a fifth significant digit. It is also found that the assumed analytical representation of the current distribution along the transverse direction does not affect the results, if the value of k_{e_l} is calculated accurately.

The end location of each $(M+1)$th and $(P+1)$th triangular weighting function does not affect the accuracy of the results if the expansion functions cover at least a quarter-wavelength from the gap discontinuity. This indicates that the higher order modes generated at the vicinity of discontinuities have highly evanescent behavior. Thus, the center of each $(M+1)$th and $(P+1)$th triangular testing function straddles the starting point of the cosine currents (see Fig. 2).

For comparison of the overall computational efficiency, the average computation times between the two methods, used to obtain the predicted results of Fig. 4 were calculated. To obtain the results of Fig. 4, the overall computation time of the proposed method is 17 times faster than that of the conventional method in [4].

Next, the scattering parameters in symmetric and asymmetric gaps were examined. Because there is a lack of data for asymmetric gaps, a symmetric gap was chosen for the initial comparison to validate the formulation and the computed results. Once the solution is validated for a symmetric gap,

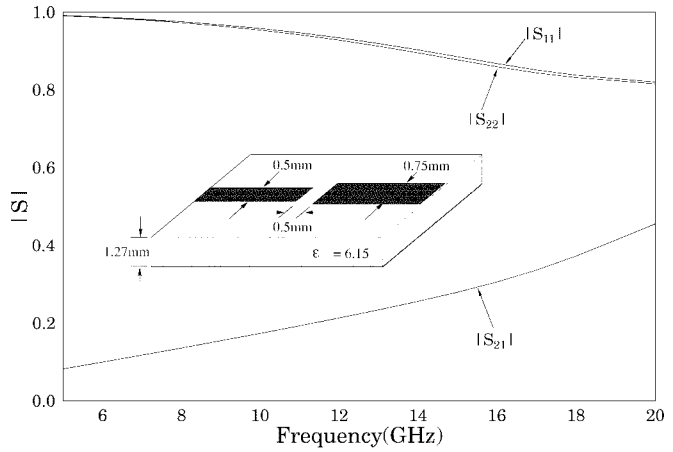

(a)

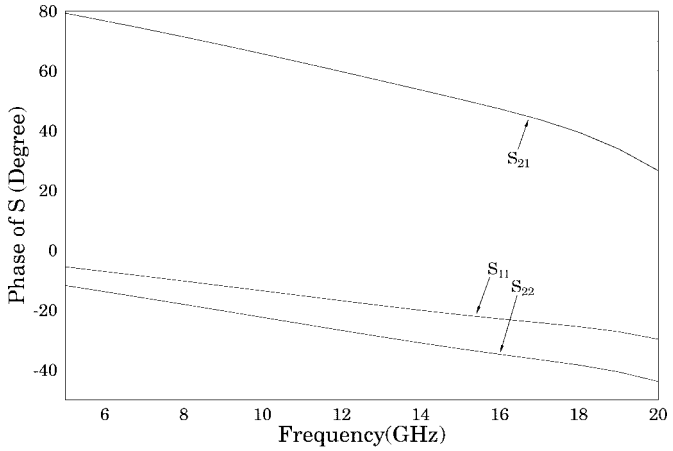

(b)

Fig. 7. S parameters of an asymmetric gap ($\epsilon_r = 6.15$, $d = 1.27$ mm, $W_1 = 0.5$ mm, $W_2 = 0.75$ mm, and $G = 0.5$ mm). (a) Magnitudes of S_{11}, S_{21}, and S_{22}. (b) Phases of S_{11}, S_{21}, and S_{22}.

one may assume that the formulation for asymmetric gaps is also correct.

The symmetric gap on a grounded dielectric slab investigated has a width $W_1 = W_2 = 0.635$ mm and gap $G = 0.508$ mm with a relative permittivity $\epsilon_r = 9.9$ and a substrate thickness $d = 0.635$ mm. The magnitude and phase of S_{11} and S_{21}, computed by using the proposed method, are compared with those of the full-wave solution [2] and are plotted in Figs. 5 and 6. Clearly, satisfactory agreement with the results of [2] has been achieved. Since the proposed results are quite similar to the full-wave data, which take into account both $\hat{x}$ and $\hat{z}$ current components, it is believed that for the gap discontinuities, the assumption of using only the longitudinal current component on the narrow microstrip line is reasonable. This is due to the fact that there is no mechanism to excite strong transverse currents for gap discontinuities. Therefore, we assume that this is valid even for asymmetric gaps if their respective strip widths remain electrically narrow. However, step–junction discontinuities (because of their current flow in the vicinity of the junctions) require the transverse current component in order to achieve sufficiently accurate results [2].

Next, the scattering parameters of an asymmetric gap for $\epsilon_r = 6.15$, $d = 1.27$ mm, $W_1 = 0.5$ mm, $W_2 = 0.75$ mm, and $G = 0.5$ mm were examined. In this case, the values of S_{11} are not equal to those of S_{22} due to the physical asymmetry with respect to the width of the two strips. The corresponding values of S_{11}, S_{21}, and S_{22} are plotted in Fig. 7 as a function of frequency. No computed or measured results for the asymmetric gap discontinuities could be found in the literature for comparison. However, based on the successful results of the symmetric gap, it can be safely assumed that the obtained results are reasonable and valid.

V. Conclusions

An efficient full-wave analysis of symmetric and asymmetric gaps is developed by using the analytical solutions for the asymptotic matrix elements. A motivation for performing such a procedure is to reduce the required computation time to evaluate the impedance-matrix elements. Analytical techniques have been successfully used to improve the computational efficiency while retaining the accuracy for the evaluation of the asymptotic matrix elements. This has been successfully demonstrated in the analysis of symmetric and asymmetric gaps.

Appendix A

In this appendix, we are concerned with the analytical solution of the following type of integral in (21):

$$B(c) = \int_0^\infty J_0(ak_y)J_0(bk_y)K_0(ck_y)\,dk_y \tag{34}$$

where J_0 is the zeroth-order Bessel function of the first kind, and K_0 is the modified Bessel function of the first kind.

With the aid of [9, formula 13.4.5.(6), p. 333], (34) can be expressed as a product of two hypergeometric series as

$$\begin{aligned} B(c) &= \int_0^\infty J_0(ak_y)J_0(bk_y)K_0(ck_y)\,dk_y \\ &= \frac{\pi}{2}\frac{1}{c}F\left(\frac{1}{2},\frac{1}{2};1;\eta\right)F\left(\frac{1}{2},\frac{1}{2};1;\zeta\right) \end{aligned} \tag{35}$$

where

$$\eta = \frac{c^2 - a^2 + b^2 - \sqrt{(c^2 - a^2 + b^2)^2 + 4a^2c^2}}{2c^2} \tag{36}$$

$$\zeta = \frac{c^2 + a^2 - b^2 - \sqrt{(c^2 + a^2 - b^2)^2 + 4b^2c^2}}{2c^2} \tag{37}$$

which is valid for any arbitrary positive values of a, b, and c.

After careful examination of (36) and (37), it is easily found that the values of η and ζ always have less than zero value, i.e., $-\infty \le \eta, \zeta \le 0$. Thus, the hypergeometric series in (35) is divergent in the region $-\infty \le \eta, \zeta \le -1$. However, these series can be transformed into geometrically convergent series (analytical region) by using the Gauss relation [10, formula 9.131, p. 1043] as

$$F\left(\frac{1}{2},\frac{1}{2};1;x\right) = \frac{1}{\sqrt{1-x}}F\left(\frac{1}{2},\frac{1}{2};1;\frac{x}{x-1}\right) \tag{38}$$

Using (38), the regions $-\infty \le \eta, \zeta \le 0$ of the hypergeometric series in (35) can be converted to analytical regions $0 < \eta/(\eta-1), \zeta/(\zeta-1) < 1$. Also, from the relations of [6, eqs. (28) and (30)], the hypergeometric series function $F(1/2, 1/2; 1; x)$ can be represented by an elliptical function as

$$F\left(\frac{1}{2}, \frac{1}{2}; 1; x\right) = \frac{2}{\pi}K(x), \qquad \text{if } 0 < x < 1 \tag{39}$$

where K is the complete elliptical function of the first kind.

With the aid of (39) and (38), $F(1/2, 1/2; 1; \eta)$ and $F(1/2, 1/2; 1; \zeta)$ can be represented by

$$\begin{aligned} &F\left(\frac{1}{2}, \frac{1}{2}; 1; \frac{c^2 - a^2 + b^2 - \sqrt{(c^2 - a^2 + b^2)^2 + 4a^2c^2}}{2c^2}\right) \\ &= \frac{\sqrt{2}c}{\sqrt{c^2 + a^2 - b^2 + \sqrt{(c^2 - a^2 + b^2)^2 + 4a^2c^2}}} \\ &\quad \times \left(\frac{2}{\pi}\right)K \\ &\quad \cdot \left(\frac{c^2 - a^2 + b^2 - \sqrt{(c^2 - a^2 + b^2)^2 + 4a^2c^2}}{-c^2 - a^2 + b^2 - \sqrt{(c^2 - a^2 + b^2)^2 + 4a^2c^2}}\right) \end{aligned} \tag{40}$$

$$\begin{aligned} &F\left(\frac{1}{2}, \frac{1}{2}; 1; \frac{c^2 + a^2 - b^2 - \sqrt{(c^2 + a^2 - b^2)^2 + 4b^2c^2}}{2c^2}\right) \\ &= \frac{\sqrt{2}c}{\sqrt{c^2 - a^2 + b^2 + \sqrt{(c^2 + a^2 - b^2)^2 + 4b^2c^2}}} \\ &\quad \times \left(\frac{2}{\pi}\right)K \\ &\quad \cdot \left(\frac{c^2 + a^2 - b^2 - \sqrt{(c^2 + a^2 - b^2)^2 + 4b^2c^2}}{-c^2 + a^2 - b^2 - \sqrt{(c^2 + a^2 - b^2)^2 + 4b^2c^2}}\right). \end{aligned} \tag{41}$$

These formulas make it possible to evaluate (35) by geometrically convergent series. Substituting (40) and (41) into (35), the closed-form solution of (34) can be obtained as follows:

$$\begin{aligned} B(c) &= \int_0^\infty J_0(ak_y)J_0(bk_y)K_0(ck_y)\,dk_y \\ &= \frac{4}{\pi}\frac{c}{\sqrt{c^2 + a^2 - b^2 + \sqrt{(c^2 - a^2 + b^2)^2 + 4a^2c^2}}} \\ &\quad \times \frac{1}{\sqrt{c^2 - a^2 + b^2 + \sqrt{(c^2 + a^2 - b^2)^2 + 4b^2c^2}}} \\ &\quad \times K\left(\frac{c^2 - a^2 + b^2 - \sqrt{(c^2 - a^2 + b^2)^2 + 4a^2c^2}}{-c^2 - a^2 + b^2 - \sqrt{(c^2 - a^2 + b^2)^2 + 4a^2c^2}}\right) \\ &\quad \times K\left(\frac{c^2 + a^2 - b^2 - \sqrt{(c^2 + a^2 - b^2)^2 + 4b^2c^2}}{-c^2 + a^2 - b^2 - \sqrt{(c^2 + a^2 - b^2)^2 + 4b^2c^2}}\right). \end{aligned} \tag{42}$$

In order to check the validity of (42), we first consider the analytical solution of the integral (34) for $a = b$. With the aid of [10, formula 6.513.2], the integral of (34) for $a = b$ can be written as

$$\begin{aligned} &\int_0^\infty J_0^2(k_y a)K_0(k_y c)\,dk_y \\ &\qquad = \frac{\pi}{2c}\left[P_{-(1/2)}\left(\sqrt{1 + \left(\frac{2a}{c}\right)^2}\right)\right]^2 \end{aligned} \tag{43}$$

where $P_{-(1/2)}$ is the spherical Legendre function of the first kind.

Using [6, eq. (30)], (43) may be expressed as a product of the following two elliptical functions:

$$\begin{aligned} &\int_0^\infty J_0^2(k_y a)K_0(k_y c)\,dk_y \\ &\qquad = \frac{4}{\pi}\frac{1}{c + \sqrt{c^2 + 4a^2}} \cdot K^2\left(\frac{\sqrt{c^2 + 4a^2} - c}{\sqrt{c^2 + 4a^2} + c}\right). \end{aligned} \tag{44}$$

It can be easily shown that (42) reduces to (44) by letting $a = b$. Thus, formula (44) can be regarded as a special case of (42) if $a = b$.

APPENDIX B

The integral $\mathcal{C}(\chi)$ in (26) over the k_x plane can be converted into an integration over the x plane by using Parseval's theorem

$$\begin{aligned} \mathcal{C}(\chi) &= \int_0^\infty \frac{\cos(k_x\chi)}{k_x^2 - k_{e_l}^2}\frac{\sin^2(k_x L_i/2)}{k_x^2}\,dk_x \\ &= \int_0^\infty F_1(k_x) \cdot F_2(k_x)\,dk_x \\ &= \pi\int_{-\infty}^\infty f_1(x) \cdot f_2(x)\,dx. \end{aligned} \tag{45}$$

Let us define $F_1(k_x) = \cos(k_x\chi)/(k_x^2 - k_{e_l}^2)$ and $F_2(k_x) = \sin^2(k_x L_i/2)/k_x^2$. With the aid of [10, formula 3.742.8], $f_1(x)$ can be solved as

$$\begin{aligned} f_1(x) &= \frac{1}{2\pi}\int_{-\infty}^\infty F_1(k_x)e^{jk_x x}\,dk_x \\ &= \frac{1}{2\pi}\int_{-\infty}^\infty \frac{\cos(k_x\chi)}{k_x^2 - k_{e_l}^2}\cos(k_x x)\,dk_x \\ &= \begin{cases} -\dfrac{1}{2k_{e_l}}\sin(|\chi|k_{e_l})\cos(|x|k_{e_l}), & |\chi| > |x| > 0 \\ -\dfrac{1}{4k_{e_1}}\sin(2|\chi|k_{e_l}), & |\chi| = |x| > 0 \\ -\dfrac{1}{2k_{e_l}}\cos(|\chi|k_{e_l})\sin(|x|k_{e_l}), & |x| > |\chi| > 0. \end{cases} \end{aligned} \tag{46}$$

Using straightforward algebraic manipulations, $f_2(x)$ can be easily written as

$$f_2(x) = \frac{1}{2\pi}\int_{-\infty}^\infty \frac{\sin^2(k_x L_i/2)}{k_x^2}\cos(k_x x)\,dk_x = \frac{L_i}{4}\Lambda\left(\frac{x}{L_i}\right) \tag{47}$$

where Λ is defined in (11).

$$\begin{aligned}\mathcal{C}(\chi) &= \pi \int_{-\infty}^{\infty} f_1(x) f_2(x)\, dk \\ &= \begin{cases} -\dfrac{\pi}{4}\dfrac{1}{k_{e_l}^3}[1-\cos(k_{e_l}L_i)]\sin(|\chi|k_{e_l}), & \text{if } |\chi| > L_i \\ -\dfrac{\pi}{4}\dfrac{1}{k_{e_l}^3}[k_{e_l}L_i - |\chi|k_{e_l} + \sin(|\chi|k_{e_l}) - \cos(k_{e_l}|\chi|)\sin(k_{e_l}L_i)], & \text{if } |\chi| < L_i \end{cases}\end{aligned} \tag{48}$$

$$\begin{aligned}\mathcal{D}(\chi) &= \int_0^{\infty} \frac{\cos(k_x\chi)}{k_x^2 - k_{e_l}^2}\sin^2(k_xL_i/2)\, dk_x \\ &= -\frac{\pi}{4k_{e_l}}\left\{\sin(k_{e_l}|\chi|) - \frac{1}{2}\sin[k_{e_l}(|\chi| + L_i)] - \frac{1}{2}\sin[k_{e_l}(||\chi| - L_i|)]\right\} \\ &= \begin{cases} -\dfrac{\pi}{4k_{e_l}}[1-\cos(k_{e_l}L_i)]\sin(k_{e_l}|\chi|), & \text{if } |\chi| > L_i \\ -\dfrac{\pi}{4k_{e_l}}[\sin(k_{e_l}|\chi|) - \sin(k_{e_l}L_i)\cdot\cos(k_{e_l}\chi)], & \text{if } |\chi| < L_i \end{cases}\end{aligned} \tag{50}$$

Substituting (46) and (47) into (45), $\mathcal{C}(\chi)$ can be evaluated exactly in closed-form in terms of sine and cosine terms as shown in (48), at the top of this page. Using [10, formula 3.727.9]

$$\int_0^{\infty} \frac{\cos(\chi k_x)}{k_x^2 - k_{e_l}^2}\, dk_x = -\frac{\pi}{2k_{e_l}}\sin(k_{e_l}|\chi|) \tag{49}$$

the integral $\mathcal{D}(\chi)$ in (27) can be expressed as shown in (50), at the top of this page, and $\mathcal{H}$ in (32) and (33) is defined as

$$\begin{aligned}\mathcal{H} &= \int_{-\infty}^{A^L} \frac{\sin(k_{e_l}|\chi|)}{|\chi - d_s|}\, d\chi + \int_{A^U}^{\infty} \frac{\sin(k_{e_l}|\chi|)}{|\chi - d_s|}\, d\chi \\ &= \int_{|A^L|+d_s}^{\infty} \frac{\sin[k_{e_l}(\chi - d_s)]}{|\chi|}\, d\chi \\ &\quad + \int_{A^U - d_s}^{\infty} \frac{\sin[k_{e_l}(\chi + d_s)]}{|\chi|}\, d\chi \\ &= \cos(k_{e_l}d_s)\int_{|A^L|+d_s}^{\infty} \frac{\sin(k_{e_l}\chi)}{\chi}\, d\chi \\ &\quad - \sin(k_{e_l}d_s)\int_{A^U+d_s}^{\infty} \frac{\cos(k_{e_l}\chi)}{\chi}\, d\chi \\ &\quad + \cos(k_{e_l}d_s)\int_{A^U-d_s}^{\infty} \frac{\sin(k_{e_l}\chi)}{\chi}\, d\chi \\ &\quad + \sin(k_{e_l}d_s)\int_{A^U-d_s}^{\infty} \frac{\cos(k_{e_l}\chi)}{\chi}\, d\chi\end{aligned} \tag{51}$$

where A^U and A^L are given by $\max[L_i, |d_s| + 10\cdot\max(W_1, W_2)]$ and $\min[-L_i, |d_s| - 10\cdot\max(W_1, W_2)]$, respectively.

Using [10, formula 3.721.1]

$$\int_0^{\infty} \frac{\sin(ax)}{x}\, dx = \frac{\pi}{2}\operatorname{sign}(a) \tag{52}$$

the infinite integral $\mathcal{H}$ in (51) can be simplified to the finite integral as

$$\begin{aligned}\mathcal{H} &= \pi\cdot\cos(k_{e_l}d_s) - \cos(k_{e_l}d_s) \\ &\quad \cdot\left[\int_0^{|A^L|+d_s} \frac{\sin(k_{e_l}\chi)}{\chi}\, d\chi + \int_0^{A^U-d_s} \frac{\sin(k_{e_l}\chi)}{\chi}\, d\chi\right] \\ &\quad + \sin(k_{e_l}d_s)\int_{A^U-d_s}^{|A^L|+d_s} \frac{\cos(k_{e_l}\chi)}{\chi}\, d\chi.\end{aligned} \tag{53}$$

ACKNOWLEDGMENT

The authors would like to thank Dr. J. F. Harvey, U.S. Army Research Office, Research Triangle Park, NC, and Dr. J. W. Mink, North Carolina State University, Raleigh, NC, for their interest and support of this work.

REFERENCES

[1] R. W. Jackson, "Full-wave, finite element analysis of irregular microstrip discontinuities," *IEEE Trans. Microwave Theory Tech.*, vol. MTT-37, pp. 81–89, Jan. 1989.

[2] N. G. Alexópoulos and S.-C. Wu, "Frequency-independent equivalent circuit model for microstrip open-end and gap discontinuities," *IEEE Trans. Microwave Theory Tech.*, vol. 42, pp. 1268–1272, July 1994.

[3] R. W. Jackson and D. M. Pozar, "Full-wave analysis of microstrip open-end and gap discontinuities," *IEEE Trans. Microwave Theory Tech.*, vol. MTT-33, pp. 1036–1042, Oct. 1985.

[4] G. W. G. Pan, J. Tan, and J. D. Murphy, "Full-wave analysis of microstrip floating-line discontinuities," *IEEE Trans. Electromag. Compat.*, vol. 36, pp. 49–59, Feb. 1994.

[5] S.-O. Park, "Analytical techniques for the evaluation of asymptotic matrix elements in electromagnetic problems," Ph.D. dissertation, Dept. Elect. Eng., Arizona State Univ., Tempe, AZ, May 1997.

[6] S.-O. Park and C. A. Balanis, "Analytical transform technique to evaluate the asymptotic part of impedance matrix of Sommerfeld-type integrals," *IEEE Trans. Antennas Propagat.*, vol. 45, pp. 798–805, May 1997.

[7] H.-Y. Yang, N. G. Alexópoulos, and D. R. Jackson, "Microstrip open-end and gap discontinuities in a substrate–superstrate structure," *IEEE Trans. Antennas Propagat.*, vol. 37, pp. 1542–1546, Oct. 1989.

[8] *The Microwave Engineer's Handbook and Buyers' Guide*. New York: Horizon, 1969, p. 72.

[9] Y. L. Luke, *Integrals of Bessel Functions*. New York: McGraw-Hill, 1962.
[10] I. S. Gradshteyn and I. M. Ryzhik, *Table of Integrals, Series, and Products*. New York: Academic, 1980.

Seong-Ook Park (S'93–M'97) was born in Kyung-Pook, Korea, in December, 1964. He received the B.S. degree from KyungPook National University, KyungPook, Korea, in 1987, the M.S. degree from Korea Advanced Institute of Science and Technology, Seoul, Korea, in 1989, and the Ph.D. degree from Arizona State University, Tempe, AZ, in 1997, all in electrical engineering.

From March 1989 to August 1993, he was an Research Engineer with Korea Telecom, Taejon, Korea, working with microwave systems and networks. He later joined the Telecommunication Research Center, Arizona State University, until his departure in September 1997. Since October 1997, he has been with the Information and Communications University, Taejon, Korea, as an Assistant Professor. His research interests include analytical and numerical techniques in the area of microwave integrated circuits and MMIC's.

Dr. Park is a member of Phi Kappa Phi.

Constantine A. Balanis (S'62–M'65–SM'74–F'86) received the B.S.E.E. degree from Virginia Polytechnic Institute and State University, Blacksburg, VA, in 1964, the M.E.E. degree from the University of Virginia, Charlottesville, in 1966, and the Ph.D. degree in electrical engineering from Ohio State University, Columbus, in 1969.

From 1964 to 1970, he was with NASA Langley Research Center, Hampton, VA. From 1970 to 1983, he was with the Department of Electrical Engineering, West Virginia University, Morgantown. Since 1983, he has been with the Department of Electrical Engineering, Arizona State University, Tempe, where he is currently Regents' Professor and Director of the Telecommunications Research Center. His research interests are in low- and high-frequency computational methods for antennas, scattering, and penetration, transient analysis, control of coupling, and reduction of pulse distortion in interconnects for monolithic microwave and millimeter-wave circuits and electronic packaging, and multipath propagation. He has authored *Antenna Theory: Analysis and Design* (New York: Wiley, 1982, 1997) and *Advanced Engineering Electromagnetics* (New York: Wiley, 1989).

Dr. Balanis is a member of ASEE, Sigma Xi, Electromagnetics Academy, Tau Beta Pi, Eta Kappa Nu, and Phi Kappa Phi. He has served as associate editor of the IEEE TRANSACTIONS ON ANTENNAS AND PROPAGATION (1974–1977) and the IEEE TRANSACTIONS ON GEOSCIENCE AND REMOTE SENSING (1981–1984) and as an editor of the *IEEE Geoscience and Remote Sensing Society Newsletter*. He served as chairman of the Distinguished Lecturer Program of the IEEE AP-S (1988–1991) and was a member of IEEE AP-S AdCom (1992–1995). He was the recipient of the 1992 Special Professionalism Award from the IEEE Phoenix Section, the 1989 IEEE Region 6 Individual Achievement Award, and the 1987–1988 Graduate Teaching Excellence Award, School of Engineering, Arizona State University.